

# Fast Scalar and Vectorial Grayscale Based Invariant Features for 3D Cell Nuclei Localization and Classification

Janina Schulz<sup>1</sup>, Thorsten Schmidt<sup>1</sup>, Olaf Ronneberger<sup>1</sup>, Hans Burkhardt<sup>1</sup>,  
Taras Pasternak<sup>2</sup>, Alexander Dovzhenko<sup>2</sup>, and Klaus Palme<sup>2</sup>

<sup>1</sup> Albert-Ludwigs-Universität Freiburg, Institut für Informatik, Lehrstuhl für  
Mustererkennung und Bildverarbeitung

<sup>2</sup> Albert-Ludwigs-Universität Freiburg, Institut für Biologie II, Botanik  
jschulz@informatik.uni-freiburg.de

**Abstract.** Since biology and medicine apply increasingly fast volumetric imaging techniques and aim at extracting quantitative data from these images, the need for efficient image analysis techniques like detection and classification of 3D structures is obvious. A common approach is to extract local features, e.g. group integration has been used to gain invariance against rotation and translation. We extend these group integration features by including vectorial information and spherical harmonics descriptors. From our vectorial invariants we derive a very robust detector for spherical structures in low-quality images and show that it can be computed very fast. We apply these new invariants to 3D confocal laser-scanning microscope images of the Arabidopsis root tip and extract position and type of the cell nuclei. Then it is possible to build a biologically relevant, architectural model of the root tip.

## 1 Introduction

Groupwise Haar integration [1] of scalar 2D and 3D images has been successfully used to classify pollen grains [2] and to segment and classify cells in tissue samples [3]. These Haar integration features are solely based on scalar values like gray value and gradient magnitude, but ignore the direction of the gradient, which is an extremely robust feature, even under varying transformations and lighting conditions. This robustness is shown by e.g. [4], who use the direction of the gradient as their main features and gain impressive results on 2D images. We extend the groupwise Haar integration framework by including vectorial gradient information and by using spherical harmonics descriptors. We furthermore show how the generalized Hough transform for spheres can be considered as a special case of our vectorial Haar integration features.

The aim of this paper is to extract the location of the cell nuclei in the Arabidopsis root tip from 3D microscope images and furthermore decide if a cell nucleus is in interphase or in a phase of mitosis. Interphase and mitosis are phases of the cell cycle, in interphase the cell nucleus is in a non-dividing state. During

mitosis the actual division into two daughter cells takes place. We concentrate on interphase (comprising more than 95% of the cells) and metaphase, which is the most characteristic phase of the different phases of mitosis. Our final aim is to build a theoretical model of the root growth, therefore it is essential to gain information about the distribution of cell divisions inside the root tip.

We are not aware of groups using image analysis on 3D microscope images of the *Arabidopsis* root tip. Still, [5] identify and track cell nuclei in 2D images of *C. elegans* embryos. But in contrast to our 3D images, the cell nuclei in [5] are well separated and can be extracted using local signal maxima. [6] use simple features and a classification tree to classify tumor cells from normal cells in 2D images.

## 2 Description of the Data

Since we intend to gain as much information as possible about the location of the cell nuclei and their phase of mitosis in *Arabidopsis thaliana*, we stain the root tips with a fluorescent dye that binds to DNA (deoxyribonucleic acid), which is mainly located inside the cell nuclei. We use DAPI (4',6-diamidino-2-phenylindole), a common fluorescent staining. The roots are taken from plants at the age of three to five days, embedded in glycerol and captured as a 3D stack with a Zeiss LSM 510 META microscope with a water objective (C-Apochromat 63x/1.2 W corr) and an excitation wavelength of 364nm. The image quality depends on the age of the roots and the preparation steps (staining and washing), but the achieved image quality is reproducible. Fig. 1 shows an example slice of one of the 3D stacks used in the experiments. Most of the cell nuclei are cells in interphase and have a roughly spherical appearance with an unstained nucleolus inside each nucleus. In metaphase, the stained part of the cell usually has the shape of a flat disk. We use images with a voxelsize of  $0.6\mu\text{m}$  (for the detection of the cell nuclei in metaphase) and of  $0.25\mu\text{m}$  for all other computations.

We first compute a series of invariant features for each voxel in the image (as presented in sec. 3), and then classify these features by use of a support-vector machine into the three classes *center of a cell nucleus in interphase*, *center of a cell nucleus in metaphase* and *no center of a cell*. Finally we visualize our results in a preliminary model of the *Arabidopsis* root tip.

## 3 Invariant Features by Groupwise Haar-Integration

Groupwise Haar integration [1] gains invariance of an image  $X$  under certain group operations by integration of a kernel function  $f$  over all these group operations:

$$I_f(X) = \int_G f(gX) dg \quad (1)$$

$G$  is the transformation group, under which the features  $I_f(X)$  should be invariant,  $g$  is one element of  $G$ . Function  $f$  computes a scalar value by a nonlinear,

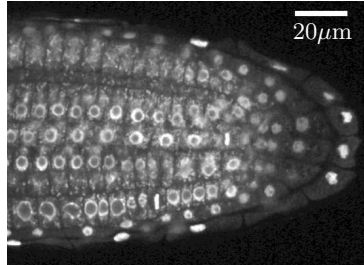


**Fig. 1.** A typical slice of a 3D microscope image of the Arabidopsis root tip. Several characteristic aspects of the data are obvious: most cell nuclei are in interphase and are characterized by a roughly spherical contour but differing heavily in intensity. Each inner cell nucleus contains a nucleolus which forms a dark sphere, a double contour arises. In the middle and in the lower part of the figure, we see two cells in metaphase (vertical bars).

but otherwise arbitrary combination of all gray values in  $X$ . As the integral is independent of the particular position and orientation of image  $X$ , the integral is invariant under  $G$ . These features can be computed either for a whole image or a subimage  $X$  (*blockwise*) or *voxelwise* for each voxel  $\mathbf{x}_0 \in X$ . In this case, we shift the origin to voxel  $\mathbf{x}_0$  and integrate over all rotations. This results in features for each voxel such that in a later classification step, all voxels are classified separately. In the upcoming sections, the features are computed voxelwise unless otherwise indicated.

### 3.1 2-Point Grayscale Invariants

A very simple, but frequently ([3],[2]) used type of kernel function are functions  $f$  with

$$f(X) = f_1(X(\mathbf{0})) \cdot f_2(X(\mathbf{r})) \quad (2)$$

where  $f_1, f_2$  are arbitrary functions on the image  $X$ , and  $X(\mathbf{0}) = X(0,0,0)$ ,  $X(\mathbf{r}) = X(0,0,r)$ ,  $r \in \mathbb{R}$ . The characteristic criterion of  $f$  is that its evaluation depends only on two points in the image. [2] shows that a fast evaluation of  $I_f(X)$  is possible using fast convolution. As functions  $f_1$  and  $f_2$  we have chosen the identity, the square root, and the exponentiation to the powers of two and three, using both, image  $X$  and gradient magnitude image  $|\nabla X|$  as an input. Radius  $r$  has been in the range of  $1\mu\text{m}$  to  $5\mu\text{m}$ . As a preprocessing step, different gaussian filters with a standard deviation between 0.05 and 4 have been applied. This can be interpreted as using a smoothed 2-point kernel function that does not depend on two points but on two gaussian regions and leads to features robust against noise.

### 3.2 Voxelwise Vector Based Grayscale Invariants

Only scalar gray value information at different positions in the image has been used with the previously described invariants. But the grayscale invariant frame-

work can be theoretically extended to include directional information [7]. We decided to use the gradient as the most important directional information and we associate every point  $\mathbf{x}$  with its gray value gradient  $(\nabla X)(\mathbf{x})$ . The general formula of a kernel function that depends on the gradient image  $\nabla X$  and is invariant under the rotation  $R$  around point  $\mathbf{x}_0$  is

$$I_f(X, \mathbf{x}_0) = \int_G f(g_R g_{\mathbf{x}_0} \nabla X) dg_R \quad (3)$$

Here  $g_{\mathbf{x}_0}$  denotes the translation of point  $\mathbf{x}_0$  to the origin and  $g_R$  operations of the rotation group  $G$ . To guarantee that  $I_f(X, \mathbf{x}_0)$  is computationally affordable, we restrain  $f$  to only depend on few values. We choose the simplest type of kernel functions, a 1-point kernel, for  $f$ :

$$f(\nabla X) = f_1(\nabla X(\mathbf{r})) \text{ with } f_1(\mathbf{u}) = \frac{\mathbf{u}}{|\mathbf{u}|} \cdot \mathbf{w} \quad (4)$$

$\mathbf{w}$  denotes a fixed unit vector,  $\cdot$  is the scalar product. Function  $f_1$  computes the scalar product of its argument with a fixed given vector (both vectors being unit vectors). The invariant  $I_f(X, \mathbf{x}_0)$  becomes

$$I_f(X, \mathbf{r}, \mathbf{x}_0) = \int_G f(g_R g_{\mathbf{x}_0} \nabla X) dg_R \quad (5)$$

$$= \int_G f_1((g_R g_{\mathbf{x}_0} \nabla X)(\mathbf{r})) dg_R \quad (6)$$

$$= \int_G \frac{(g_R g_{\mathbf{x}_0} \nabla X)(\mathbf{r})}{|(g_R g_{\mathbf{x}_0} \nabla X)(\mathbf{r})|} \cdot \frac{\mathbf{r}}{|\mathbf{r}|} dg_R \quad (7)$$

We now consider the special case of Euclidean coordinates and thus integrate over all rotation matrices  $R$ . The inverse matrix  $R^{-1}$  undoes the rotation of the gradients under rotation of the image  $X$ . This is a major difference to the computation of grayscale invariants on images with only scalar values. Here  $O_3$  is the group of all rotation matrices.

$$I(X, \mathbf{r}, \mathbf{x}_0) = \int_{O_3} R^{-1} \frac{(\nabla X)(R \mathbf{r} - \mathbf{x}_0)}{|(\nabla X)(R \mathbf{r} - \mathbf{x}_0)|} \cdot \frac{\mathbf{r}}{|\mathbf{r}|} dR \quad (8)$$

This invariant is a strong measurement for how spherical given structures around point  $\mathbf{x}_0$  are as it accumulates gradients that show in radial direction towards  $\mathbf{x}_0$ . We use this as a basic detector for the roughly spherical cell nuclei in interphase. As only nonlinear kernel functions are able to distinguish between complex equivalence classes, we include another highly nonlinear component to our invariant, that improves results significantly. We choose a peak-like gaussian function  $G_\sigma$  as a nonlinear weight of the scalar product, applied before integration.

Our invariant only uses unit vectors and thus dismisses all information about how strong the gradients are. As a result, the feature is independent of the strength of the edges and of the gray value. This is mostly desired, as the contours differ markedly in strength. Thus we explicitly do not weight the summands

with the gradient magnitude, yet we decided to include the absolute gray value  $X(R \mathbf{r} - \mathbf{x}_0)$  as a factor. So, we avoid detecting dim and high-frequency noise and at the same time emphasize cell nuclei with a comparably bright, but very soft contour. Finally, we compute the invariant on both the original image and the inverted image to utilize both, the contour of the cell nucleus and the inner contour of the nucleolus.

The integration over all rotation matrices is impractical for large images, because it has to be evaluated for all points  $\mathbf{x}_0 \in X$  and all possible radii  $|\mathbf{r}|$ . [7] avoids this problem by computing the integral only for a small, mostly random subset of all points, but this is only reasonable if the data is already segmented. Thus we developed a very fast method to approximate eq. (8) combined with a gaussian peak and compute  $I(X, \mathbf{r}, \mathbf{x}_0)$  for all points  $\mathbf{x}_0 \in X$  and for a set of  $m$  different radii  $|\mathbf{r}_i|$  in  $O(|X| \cdot m)$ .

**Fast Computation of Vector Based Grayscale Invariants.** In eq. (8) combined with a gaussian peak only very few of the summands contribute significantly to the integral. We use this sparseness to reduce computation time tremendously by changing the evaluation order. We do not compute the integral over all rotation matrices for all  $(\mathbf{r}, \mathbf{x}_0)$  sequentially, but we consider for each point  $\mathbf{x}_i \in X$  all integrals  $I(X, \mathbf{r}, \mathbf{x}_0)$  to which  $\mathbf{x}_i$  contributes significantly. The respective contribution of each point  $\mathbf{x}_i$  can be accumulated easily for each integral  $I(X, \mathbf{r}, \mathbf{x}_0)$  at once by introducing a voting scheme based on an iteration over all gradients. Therefore, for every voxel  $\mathbf{x}_i$  with associated gradient  $(\nabla X)(\mathbf{x}_i)$  and for every possible radius  $r$ , we vote for the coordinates  $(x, y, z)$  of the point  $\mathbf{v}$  that lies in direction of the gradient at distance  $r$  from  $\mathbf{x}_i$ , as this point is the main contributor to the integral. This results in a four-dimensional parameter space  $V(x, y, z, r)$  that reflects how strong a perfect sphere with radius  $r$  is expressed around position  $\mathbf{v} = (x, y, z)$ . Afterwards  $V(x, y, z, r)$  is smoothed with a four-dimensional gaussian filter to become robust against disturbances of the spherical structure. That way we take the gaussian distribution applied to eq. (8) into account. It is not strictly equivalent but includes a smoothing in direction of the radius, which is not given in eq. (8) but desired. As a result, local maxima reflect centers of spheres. They are found by sequentially extracting global maxima and setting the neighborhood defined by radius  $r$  in  $V(x, y, z, r)$  to zero. Using a divide & conquer approach it is possible to extract  $k$  maxima in  $O(N + r_{\max} \cdot \log N/d)$  instead of the naive  $O(kN)$ , what makes the effort for extraction of maxima negligible compared to the invariant computation. During accumulation of the votes in  $V(x, y, z, r)$  it is possible to skip very low gradients and thus reduce computation time even more without worsening the results.

Regarding this computation method it becomes obvious that the 1-point vector based grayscale invariants form basically a generalized Hough transform (GHT) [8] for spheres. The generalized Hough transform usually considers the angle between the gradient at a point  $\mathbf{x}_i$  and the vector from  $\mathbf{x}_i$  to a point of reference (center) and maintains a memory-intensive lookup table. This is what eq. (8) implicitly does, but it is outperformed with respect to both, time and memory, by the use of the gaussian  $G_\sigma$  and the fast computation method.

Thus we have shown, that the generalized Hough transform for spheres can be considered as a special case of vectorial grayscale invariants, namely of those with the simple 1-point kernel of eq. (4). The ability to discriminate between complex equivalence classes increases with the complexity of the kernel function, especially 2- and 3-point kernel functions are more powerful than 1-point kernel functions. Thus the vectorial grayscale invariants form a very powerful framework embedding the robustness of the GHT.

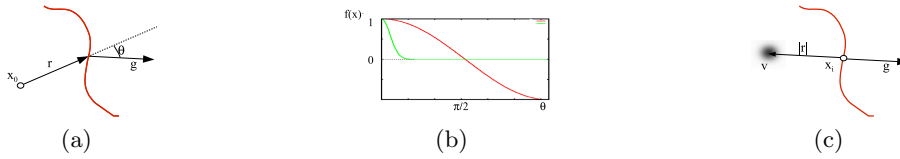


**Fig. 2.** Fig. (a) visualizes eq. (8). Starting from a base point  $\mathbf{x}_0$  (i.e. a potential center of a cell nucleus) the scalar product between vector  $\mathbf{r}$  and gradient  $\mathbf{g}$  is computed. Fig. (b) shows how the scalar product would behave against the angle  $\theta$  between  $\mathbf{r}$  and  $\mathbf{g}$  (red), whereas the weighting with a gaussian function (green) assures that only small  $\theta$  near 0 contribute to the integral. In fig. (c) the fast computation method (sec. 3.2) is illustrated. At every point  $\mathbf{x}_i$  a smoothed vote is given for the point  $\mathbf{v}$  that lies in opposite direction of the gradient  $\mathbf{g}$  at distance  $|\mathbf{r}|$ . Comparing fig. (a) and (c) it becomes obvious how the fast computation method inverts the evaluation steps.

### 3.3 Spherical Harmonics Descriptors

An additional set of invariants is computed by using spherical harmonics descriptors [9]. We expand the gray values on spheres around certain points  $\mathbf{x}_0$  in spherical harmonics and determine the bandwise distribution of the signal energy. These spherical harmonics descriptors can easily be embedded in the Haar integration framework.

Every function  $f$  in spherical coordinates  $(\theta, \phi, \rho)$  that does not depend on  $\rho$  can be expanded in a series of spherical harmonics  $Y_l^m(\theta, \phi)$ :

$$f(\theta, \phi) = \sum_{l=0}^{\infty} \sum_{m=-l}^l C_l^m \cdot Y_l^m(\theta, \phi) \quad (9)$$

The coefficients  $C_l^m$  are computed by a projection of function  $f$  onto the basis:

$$C_l^m = \int f(s) Y_l^{m*}(s) ds \quad (10)$$

To gain rotation invariant features we expand at every point  $\mathbf{x}_0$  a sphere with radius  $r$  in spherical harmonics and analyse the bandwise fraction of the total

signal energy for each band  $l$ . The operation  $g_r$  denotes a scaling of the sphere to radius  $r$ :

$$I(l, r, \mathbf{x}_0) = \frac{\left( \sum_{m=-l}^l \int X(\mathbf{x}) \cdot (g_{\mathbf{x}_0} g_r Y_l^{m*})(\mathbf{x}) d\mathbf{x} \right)^2}{\int X^2(\mathbf{x}) \cdot (g_{\mathbf{x}_0} g_r Y_0^{0*})(\mathbf{x}) d\mathbf{x}} \quad (11)$$

This can be considerably simplified as the spherical harmonics form an orthogonal basis:

$$I(l, r, \mathbf{x}_0) = \frac{\sum_{m=-l}^l \left( \int X(\mathbf{x}) \cdot (g_{\mathbf{x}_0} g_r Y_l^{m*})(\mathbf{x}) d\mathbf{x} \right)^2}{D + \int X^2(\mathbf{x}) \cdot (g_{\mathbf{x}_0} g_r Y_0^{0*})(\mathbf{x}) d\mathbf{x}} \quad (12)$$

The denominator reflects the total signal energy of the sphere to which we add a denoising term  $D$  to become robust against small energy peaks (i.e. noise). The invariant of band  $l = 2$  is particularly well suited to characterize the flat disk shape of cells in metaphase. We evaluated only band 2 on spheres with radii up to  $3.5\mu\text{m}$  and a series of gaussian preprocessing filters with standard deviations of 0.03, 0.15 and 0.27. For  $D$  it has proven sensible to use a value almost in the region of the total energy.

**General Spherical Invariants.** Another set of invariants that helped to describe the cell nuclei are what we named general spherical invariants. They can also be expressed as a Haar integration kernel and they are a generalization of 2-point grayscale invariants, pseudo 3-point invariants, see [3], and spherical harmonics descriptors. They can be computed according to

$$I_{f_1, f_2, f_3}(X, \mathbf{x}_0, r, l) = f_1(X(\mathbf{x}_0)) \cdot f_2 \left( \sum_{m=-l}^l \left( \int f_3(X) \cdot (g_{\mathbf{x}_0} g_r Y_l^m)(\mathbf{x}) d\mathbf{x} \right)^2 \right)$$

Here,  $f_1, f_2, f_3$  are transformations on image  $X$ , e.g. pointwise exponentiation to different exponents. This possibility to include a variety of nonlinear transformations is one advantage of these invariants. We evaluated band 0, 1, 2, 3 and 4 with radii up to  $5.5\mu\text{m}$  and functions  $f_1(X) = X$  and  $f_{2,3}(X) = \sqrt{X}$  after applying a gaussian smoothing filter (with  $\sigma \in \{0.06, 0.18, 0.3\}$ ).

### 3.4 Radius and Gray Value Cooccurrence Matrices

Our classification results can be further improved by including an explicit measurement how gray values are distributed in a local region around point  $\mathbf{x}_0$ . Therefore we build a two-dimensional matrix for every voxel  $\mathbf{x}_0$  with entries of the absolute number of voxels with gray value  $g_i$  at distance  $r_i$  to point  $\mathbf{x}_0$ . For the gray values we use five bins and eight for the radii up to  $9\mu\text{m}$ . The radius and gray value cooccurrence matrix is computed with input images  $X$  and  $|\nabla X|$ . Furthermore we use the minimal, maximal and average distance of all bright points, i.e. points with at least 80% of the maximal gray value in a local region around point  $\mathbf{x}_0$  in the gaussian smoothed image  $G_\sigma(X)$ , and their

standard deviation as features. Another small subset of our features compute the square root of the sum of all points in distance  $r$  from point  $\mathbf{x}_0$  in images  $X$  and  $|\nabla X|$ . Radius  $r$  is chosen between  $0.6\mu\text{m}$  and  $12.0\mu\text{m}$ , and as a preprocessing step, gaussian filters of standard deviation  $\sigma = 0.03$  and  $0.18$  are used.

### 3.5 Evaluation of the Features

Our aim is to classify each voxel as being a central point of either a cell in interphase or a cell in metaphase or none of it. To reach this with a minimal effort of computing time we divide the process into two steps:

1. Detection of the cell nuclei in interphase
  - (a) Evaluation of the vector based grayscale invariants (sec. 3.2). They are a very good estimate for the position of cell nuclei in interphase as they detect spherical structures.
  - (b) To verify these hypotheses for cell nuclei in interphase, we compute further blockwise invariants in a local spherical subimage around the maxima detected in step 1 (according to sections 3.1, 3.4).
  - (c) The invariants are used as features by a support-vector machine (SVM) to classify the subimages into two classes *cell nucleus* and *not a cell nucleus*.
2. Detection of the cell nuclei in metaphase
  - (a) The invariants from sec. 3.1 and 3.3, the original image and gradient magnitude images smoothed with gaussian filters are used as voxelwise features. A support-vector machine classifies each voxel into one of the classes *centers of cells in a mitosis phase* and *other voxels*

We use a two-class support-vector machine with a gaussian kernel with parameters  $\gamma = 0.001$  and  $\text{cost} = 10$ . These parameters were selected by a grid search done on a large range of  $\gamma$  and the cost factor.

## 4 Experiments and Discussion

The invariants are selected and optimized for the localization and classification of cell nuclei in 3D confocal laser-scanned microscope images of the Arabidopsis root tip. For evaluation we chose five 3D image stacks from five different plants, computed the invariant features, trained the support-vector machine with two of the stacks and used the three remaining stacks as strictly separated test sets.

Our quantitative results in table 1 and fig. 3 show that a sensible model can be built with the information extracted by our invariants. It has been possible to classify over 80% of the cell nuclei correctly. It is not relevant if we miss some of the cell nuclei in interphase, but it is important to retrieve enough information about the location of these cell nuclei that it is possible to define the architecture of the Arabidopsis root tip, this means to identify the different cell files (fig. 3). We have easily reached this aim. For the biological research concerning root growth it is important that as few cell nuclei in metaphase as possible are missed.

This allows us to draw conclusions about the statistical distribution of dividing cells given a sufficient amount of data sets. The fact, that only one cell nucleus in metaphase has been missed in only one test set is a very strong result. It allows us to rely on the total recall of the cell nuclei in metaphase. If full precision is needed, a human interactor only has to double check for false positives in the very small-sized set of localized cell nuclei. These quantitative results can easily be visualized in a 3D model of the root tip (fig. 3 (a), (b)). Each sphere corresponds to one detected cell nucleus. The coloration of the spheres is according to their distance from the hull of the root tip. This allows to distinguish between the different cell files and to identify the cellular architecture of the root tip. Figure 3 (c) shows a slice of the original 3D microscope image. We have marked the cell nuclei detected by our invariants.

**Table 1.** Quantitative results. We show the confusion tables of the voxelwise classification of the voxels in three test sets of whole Arabidopsis root tips from different plants. Another two data sets from different plants have been used as training sets. The results show that it has been possible to extract most of the cells in interphase (I.). They are needed to gain information about the architecture of the Arabidopsis root tip. Furthermore it has been possible to detect all cell nuclei in metaphase (M.), except one in one test set. They are the crucial information for a biological analysis of the root growth. In the case of missed centers in interphase, we distinguish between cell centers missed by our vector invariants (sec. 3.2) and cells missclassified by the SVM, the sums in the confusion tables represent that. The class of voxels that are not the center of a cell in interphase or metaphase is abbreviated to *no c.* for *no center*.

	classified as				classified as				classified as		
	no c.	I.	M.		no c.	I.	M.		no c.	I.	M.
no c.	$8 \cdot 10^7$	37	1	no c.	$8 \cdot 10^7$	32	1	no c.	$8 \cdot 10^7$	34	4
I.	184+26	<b>934</b>	0	I.	232+39	<b>1009</b>	0	I.	255+37	<b>962</b>	0
M.	1	0	<b>12</b>	M.	0	0	<b>5</b>	M.	0	0	<b>10</b>

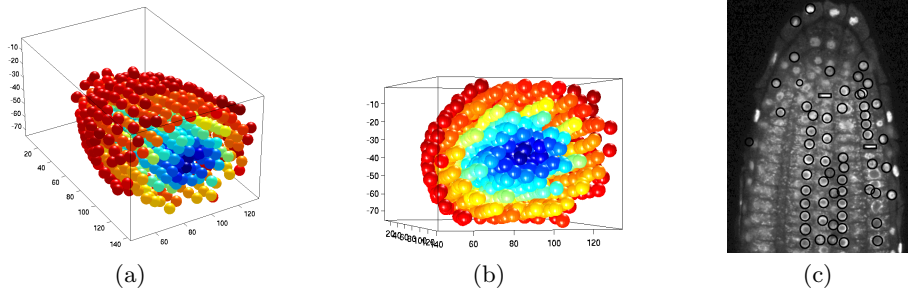


**Fig. 3.** Visualization of the results. Each sphere represents a cell nucleus we detected. The cellular architecture is clearly visible in fig. (a) and (b) as the cells form long strands towards the tip. In the example slice in fig. (c) the detected cells in interphase are marked with a circle, the cells in metaphase with a box.

## 5 Conclusion and Further Work

This paper introduces a composition of partly new invariant features that are based on grayscale invariants. The established scalar grayscale invariants have been significantly extended to include vectorial information. In particular we have shown how a robust detector for spherical structures can be derived from vectorial invariants and how it can be computed very fast.

We apply our set of invariants to laser-scanned 3D images of Arabidopsis root tips where the cell nuclei have been stained. We correctly classify about 80% of the cell nuclei in interphase and have succeeded in building an architectural model of the root tip. No tedious manual counting and/or segmentation of the cells in 3D stacks is required any more to analyze the cellular arrangement.

Furthermore we have very reliably localized the cells in metaphase (near 100% recall), which is crucial for further research in the field of Arabidopsis root growth. To measure growth at a cellular level, we need a strong, quantitative indicator, where cell division takes place.

An automated large-scale evaluation of 3D Arabidopsis microscope images based on the work done is planned for the near future. Further work will include microscope images of plants marked with green fluorescent proteins (GFP), these gene expressions are able to color exactly one or two of the cell files. This simplifies the classification of the cell nuclei into these cell files enormously and thus a more stable analysis of the file-based distribution of the cell nuclei is possible.

## References

1. Schulz-Mirbach, H.: Invariant features for gray scale images. DAGM-Symposium, Bielefeld, Germany (1995)
2. Ronneberger, O., et al.: General-purpose object recognition in 3d volume data sets using gray-scale invariants. ICPR, Quebec, Canada (2002)
3. Fehr, J., et al.: Self-learning segmentation and classification of cell-nuclei in 3d volumetric data using voxel-wise gray-scale invariants. DAGM-Symposium, Vienna, Austria (2005)
4. Lowe, D.G.: Distinctive image features from scale-invariant keypoints. *Int. J. of Computer Vision*, 60, 2 (2004)
5. Bao, Z., et al.: Automated cell lineage tracing in caenorhabditis elegans. *PNAS* (2006)
6. Wirjadi, O., et al.: Automated feature selection for the classification of meningioma cell nuclei. *Bildverarbeitung für die Medizin* (2006)
7. Reiser, M., et al.: General purpose invariant 3d features based on group integration using directional information and spherical harmonic expansion. ICPR, Hong Kong (2006)
8. Ballard, D.: Generalizing the hough transform to detect arbitrary shapes. *Pattern Recognition*, 13(2) (1981)
9. Kazhdan, M., et al.: Rotation invariant spherical harmonic representation of 3d shape descriptors. *Symp. on Geom. Process.* (2003)